the FEBS Journal

Crystal structures of two tetrameric β-carbonic anhydrases from the filamentous ascomycete *Sordaria macrospora*

Ronny Lehneck[1], Piotr Neumann[2], Daniela Vullo[3], Skander Elleuche[4], Claudiu T. Supuran[3,5], Ralf Ficner[2] and Stefanie Pöggeler[1]

1 Institute of Microbiology and Genetics, Department of Genetics of Eukaryotic Microorganisms, Georg-August-University Göttingen, Germany
2 Institute of Microbiology and Genetics, Department of Molecular Structural Biology, Georg-August-University Göttingen, Germany
3 Dipartimento di Chimica Ugo Schiff, Università degli Studi di Firenze, Sesto Fiorentino, Florence, Italy
4 Institute of Technical Microbiology, Hamburg University of Technology, Germany
5 Neurofarba Department, Section of Pharmaceutical and Nutriceutical Sciences, Università degli Studi di Firenze, Sesto Fiorentino, Florence, Italy

Keywords
carbon dioxide; crystal structure; enzyme inhibition; *Sordaria macrospora*; β-class carbonic anhydrase

Correspondence
S. Pöggeler, Institute of Microbiology and Genetics, Department of Genetics of Eukaryotic Microorganisms, Georg-August-University Göttingen, Grisebachstr. 8, 37077 Göttingen, Germany
Fax: +49 551 39 10123
Tel: +49 551 39 13930
E-mail: spoegge@gwdg.de

This paper is dedicated to Professor Karl Esser (Bochum) on the occasion of his 90th birthday.

(Received 16 December 2013, revised 30 January 2014, accepted 31 January 2014)

doi:10.1111/febs.12738

Carbonic anhydrases (CAs) are metalloenzymes catalyzing the reversible hydration of carbon dioxide to bicarbonate (hydrogen carbonate) and protons. CAs have been identified in archaea, bacteria and eukaryotes and can be classified into five groups (α, β, γ, δ, ζ) that are unrelated in sequence and structure. The fungal β-class has only recently attracted attention. In the present study, we investigated the structure and function of the plant-like β-CA proteins CAS1 and CAS2 from the filamentous ascomycete *Sordaria macrospora*. We demonstrated that both proteins can substitute for the *Saccharomyces cerevisiae* β-CA Nce103 and exhibit an *in vitro* CO_2 hydration activity (k_{cat}/K_m of CAS1: 1.30×10^6 $M^{-1} \cdot s^{-1}$; CAS2: 1.21×10^6 $M^{-1} \cdot s^{-1}$). To further investigate the structural properties of CAS1 and CAS2, we determined their crystal structures to a resolution of 2.7 Å and 1.8 Å, respectively. The oligomeric state of both proteins is tetrameric. With the exception of the active site composition, no further major differences have been found. In both enzymes, the Zn^{2+} -ion is tetrahedrally coordinated; in CAS1 by Cys45, His101 and Cys104 and a water molecule and in CAS2 by the side chains of four residues (Cys56, His112, Cys115 and Asp58). Both CAs are only weakly inhibited by anions, making them good candidates for industrial applications.

Database
Structural data have been deposited in the Protein Data Bank database under accession numbers 4O1J for CAS1 and 4O1K for CAS2.

Structured digital abstract
- CAS1 and CAS2 bind by x-ray crystallography (View interaction)

Introduction

The gas carbon dioxide (CO_2) can be considered as a key molecule in the life of all organisms. It is the end product of respiration in heterotrophic organisms and the raw material for the biosynthesis of carbohydrates by autotrophic organisms. In addition to its metabolic functions, CO_2 can also act as a mediator triggering

Abbreviations
CA, carbonic anhydrase; MTS, mitochondrial target sequence; PDB, Protein Data Bank; SD, synthetic dextrose; SG, synthetic galactose; YPD, yeast extract, peptone, dextrose.

animal behavior and the virulence of pathogenic organisms [1–6]. In nature, CO_2 is reversibly hydrated by the reaction $CO_2 + H_2O \leftrightarrow HCO_3^- + H^+$. Bicarbonate ($HCO_3^-$), the hydration product of CO_2, is an important metabolite involved in many biosynthetic reactions [7–9]. The spontaneous and balanced interconversion of CO_2 and bicarbonate is slow but can be accelerated by the enzyme carbonic anhydrase (CA). Usually, CAs are Zn^{2+} -dependent metalloenzymes, although CAs harboring a Cd^{2+} or Fe^{2+} ion at their active site also have been described [10,11]. These enzymes can be identified in all three domains of life and are considered to be the result of convergent evolution. CAs can be divided into five classes (α, β, γ, δ and ζ) that are unrelated in amino acid sequence and structure [7,12,13]. The β-class can be further subdivided into plant-type and cab-type subclasses [14,15]. Subsequent to the discovery of the first CA in 1933 [16], the α-class has received the most attention. At least 16 different α-CA isoforms are encoded in mammals [17] and these have been shown to be involved in pH regulation, transport of CO_2 and electrolyte secretion [18,19]. Determination of the crystal structure of the α-CA isozymes I, II, III, IV, V, VI, IX, XII, XIII and XIV has revealed a high degree of structural similarity [20–22]. The typical fold of α-CAs is characterized by a central antiparallel β-sheet harboring the active site, which is located in a large cone-shaped cavity that reaches the center of the protein molecule. The Zn^{2+} ion, essential for catalysis, is located close to the bottom of the cavity. It is coordinated by three conserved histidine residues in a tetrahedral geometry with H_2O or OH^- as the fourth ligand.

In the large fungal kingdom, α-CAs play only a minor role and the majority of fungi encode at least one β-CA. The genomes of basidiomycetous and hemiascomycetous yeasts contain only β-CAs, whereas most filamentous ascomycetes encode multiple β-CAs and also possess genes encoding α-class CAs. Various gene duplication and gene loss events during evolution appear to be the cause for the multiplicity of CAs in fungi. In filamentous ascomycetes, a gene encoding a plant-type β-CA was duplicated, resulting in two closely-related isoforms differing with respect to the presence or absence of an N-terminal mitochondrial target sequence (MTS) [23]. Recent work demonstrates that fungal β-CAs are important for CO_2 sensing in fungal pathogens, as well as for the regulation of sexual development [2,24,25]. Despite the large number of fungal β-CAs that are known, only two have been structural characterized to date: the N-terminally truncated *Saccharomyces cerevisiae* CA Nce103 and the full-length CA Can2 from the basidiomycete *Cryptococcus neoformans* [26,27]. Both enzymes exhibit *in vitro* activity and are essential for growth under ambient air [2,9,28,29]. The crystal structures of *S. cerevisiae* and *C. neoformans* β-CAs resemble structures of plant-type β-CAs and consist of an N-terminal arm, a conserved α/β core and a C-terminal subdomain [26,27]. The zinc ion is coordinated tetrahedrally by two cysteine and one histidine residue, whereas the fourth position is occupied by a water molecule. Major structural differences between the fungal β-CAs were identified within the N-terminal extension. Can2 has an unusual N-terminal extension that is apparently important for enzymatic activity. Inhibition studies revealed that Can2 and Nce103 are strongly inhibited by sulfonamides and anions [30,31].

Previously, we showed that four different CA-genes (*cas1*, *cas2*, *cas3* and *cas4*) are encoded in the genome of the filamentous ascomycete *Sordaria macrospora* [23,32]. CAS1 and CAS2 are closely-related proteins that belong to the plant-like subgroup of β-CAs, whereas *cas3* encodes a cab-type enzyme and *cas4* encodes an α-class protein. Based on the similarity of *cas1* and *cas2*, these genes are proposed to be the result of an ancient gene duplication event [23]. CAS1 is a cytoplasmic enzyme, whereas CAS2 exhibits a signal peptide for translocation into the mitochondria. Both enzymes are involved in sexual development and are proposed to be the major CAs in *S. macrospora* [8]. The present study comprised a biochemical and structural characterization of CAS1 and CAS2 from *S. macrospora*. Both *cas1* and *cas2* were capable of substituting for *NCE103* when heterologously expressed in the Δ*nce103* deletion mutant. Recombinant *cas1* and *cas2* expressed in *Escherichia coli* displayed CO_2 hydration activity *in vitro*. Crystal structures of CAS1 and CAS2 revealed a tetrameric oligomerization state, comprising the first examples of tetrameric β-CAs in the fungal kingdom.

Results

S. macrospora cas1 and *cas2* complement the yeast deletion mutant Δ*nce103*

Heterologous expression of CA genes rescues the *S. cerevisiae* Δ*nce103* deletion mutant [29], with complementation depending on carbonic anhydrase activity of the heterologous enzyme [33]. To demonstrate the ability of CAS1 and CAS2 to functionally restore the CA-deficient yeast strain, both genes were expressed in the haploid deletion strain CEN.HE28-h (Table S1). The full-length cDNA of *cas1* and a truncated version of the *cas2* cDNA, lacking the mitochondrial target

sequence, fully complemented the phenotype of the *S. cerevisiae* Δ*nce103* CA mutant, demonstrating the carbonic anhydrase activity of CAS1 and CAS2 (Fig. 1). The haploid deletion strain transformed with the empty vector served as negative control, whereas the heterozygous strain (CEN.HE28) transformed with the empty vector was used as a positive control. In addition, all strains were tested for their viability at 5% CO_2. To verify the production of both proteins, western blotting with anti-His serum was performed (Fig. 1).

Heterologous expression in *E. coli*, purification and enzyme activity

CAS1 is a cytosolic protein composed of 234 amino acids with a calculated molecular weight of 25.1 kDa. The native 284 amino acids CAS2 protein exhibits an N-terminal signal peptide for translocation into mitochondria [8]. The mitochondrial target sequence (MTS) is predicted to be cleaved between His59 and Ser60 [23]. Therefore, the nucleotides encoding the MTS were removed to enable expression of *cas2* in *E. coli*. The *cas2* gene expressed in *E. coli* encodes a protein of 225 residues with a calculated molecular weight of 25.9 kDa. CAS1 and CAS2 were synthesized in *E. coli* Rosetta (DE3) cells as N- and C-terminal His-tagged fusion proteins, respectively. After purification, 5–10 mg of CAS1 and 10–20 mg of CAS2 could be obtained per litre of culture.

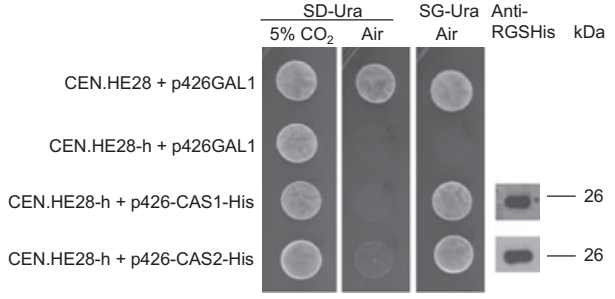

Fig. 1. Functional complementation of the haploid *S. cerevisiae* CA deletion mutant with *cas1* and *cas2* of *S. macrospora*. The haploid yeast deletion strain CEN.HE28-h was only able to grow under elevated 5% CO_2 conditions. It was transformed with galactose inducible plasmids p426-CAS1-His and p426-CAS2-His, which express either *cas1* or *cas2*. Recombinant strains were grown in a 5% CO_2 enriched atmosphere as viability control and at ambient air on SD-Ura and SG-Ura plates for repression and induction of gene expression. As controls, the haploid, as well as the heterozygous diploid strain (CEN.HE28), were transformed with the empty vector p426GAL1. Complementation was confirmed when growth occured under ambient air on SG-Ura plates. Western blotting with anti-His serum (Qiagen, 1 : 4000, 1 × NaCl/P_i + 0.5% BSA) was performed to confirm the production of the proteins.

The enzymes were concentrated to 10 mg·mL^{-1} and dialyzed against 50 mM Hepes (pH 8.3), 50 mM NaCl, and tested in a stopped-flow CO_2 hydration assay as described in the Materials and methods. Both enzymes exhibited measurable *in vitro* CO_2 hydration activity (k_{cat}/K_m of CAS1: 1.30 × 10^6 M^{-1}·s^{-1}; CAS2: 1.21 × 10^6 M^{-1}·s^{-1}) (Table 1). In addition, CAS1 and CAS2 were only weakly inhibited by the widely used sulfonamide drug acetazolamide, with inhibition constants of 445 nM and 816 nM against CAS1 and CAS2, respectively. Inhibition by anions was also investigated because these have been shown to effectively inhibit CA activity [34]. The majority of the anions tested were ineffective at inhibiting CAS1 and CAS2 (Table 2).

Perchlorate and tetrafluoroborate showed weak inhibition, similar to several other CAs [35]. Nitrite and nitrate anions were also ineffective CAS1 and CAS2 inhibitors with inhibition constants over 100 mM. The halogens bromide and chloride inhibited CAS1 with inhibition constants of 9.3 and 9.2 mM, respectively, whereas CAS2 was inhibited less efficiently. Conversely, CAS2 was more strongly inhibited by sulfate (K_I = 4.8 mM) than was CAS1 (K_I > 100 mM). The best anionic inhibitors for both CAS1 and CAS2 were sulfamide, sulfamate, phenylboronic acid and phenylarsonic acid, with inhibition constants in the range 84–9 μM.

Structural features of CAS1 and CAS2

To determine the structural details of both enzymes, we crystallized CAS1 and CAS2 and solved their three-dimensional structures (Table 3). CAS1 crystallized in space group $P2_12_12_1$ with two monomers occupying the asymmetric unit. The structure was refined at 2.7 Å to crystallographic R factors of 20.4% and 25.1% for R_{work} and R_{free}, respectively. Analysis of crystal contacts using the PISA [36] suggested that the biologically active molecule is a homotetramer possessing D_2 symmetry (Fig. 2A). CAS2 crystallized in the F222 space group with one monomer occupying the asymmetric unit, and the structure was refined at 1.8 Å to a final R_{work} of 19.1% and R_{free} of 21.1%. Crystal contact analysis indicated an equivalent homotetrameric oligomerization state to CAS1 (Fig. 2B). The final CAS1 and CAS2 models comprise protein residues 4–213 and 14–224, respectively. The missing residues (CAS1: 1–3, 214–234; CAS2: 1–13, 225) could not be localized in the electron density map and are most likely disordered. Size exclusion chromatography and multi-angle laser light scattering confirmed that both enzymes are also homotetrameric in solution

Table 1. Kinetic parameters for the CO_2 hydration reaction catalyzed by the human cytosolic isozymes hCA I and II (α-class CAs) at 20 °C and pH 7.5 in 10 mM Hepes buffer and 20 mM Na_2SO_4, and the β-CAs Can2, CalCA from *C. neoformans* and *C. albicans*, respectively. SceCA (from *S. cerevisiae*), the plant *Flaveria bidentis* CA (FbiCA 1) and CAS1 and CAS2 of *S. macrospora* measured at 20 °C (pH 8.3) in 20 mM Tris buffer and 20 mM $NaClO_4$. Inhibition data with the clinically used sulfonamide acetazolamide (5-acetamido-1,3,4-thiadiazole-2-sulfonamide) are also provided.

Isozyme	Activity level	k_{cat} (s^{-1})	k_{cat}/K_m ($M^{-1}\cdot s^{-1}$)	K_I (acetazolamide) [nM]
hCA I	Moderate	2.0×10^5	5.0×10^7	250
hCA II	Very high	1.4×10^6	1.5×10^8	12
Can2	Moderate	3.9×10^5	4.3×10^7	10.5
CalCA	High	8.0×10^5	8.0×10^5	132
SceCA	High	9.4×10^5	9.8×10^7	82
FbiCA 1	Low	1.2×10^5	7.5×10^6	27
CAS1	Low	1.2×10^4	1.30×10^6	445
CAS2	Low	1.3×10^4	1.21×10^6	816

(data not shown). The monomers of CAS1 and CAS2 are structurally highly similar; the calculated root mean square deviation (rmsd) amounts to 1.63 Å and has been calculated for 185 matched Cα atoms, of which 84 are identical in sequence (Fig. 3). The overall structure of each monomer consists of an N-terminal region forming a long arm composed of two perpendicularly oriented α-helices (α1 and α2) spanning the adjacent subunit and thus facilitating dimer formation. The central core is made up of a five-stranded mixed β-sheet (β1–β5), of which four β-strands (β2–β1–β3–β4) are in a parallel arrangement and the fifth (β5) is antiparallel (Fig. 3). The active center is composed mostly of residues located at the tips of β-strands: β1 (Cys45 of CAS1 and Cys56 of CAS2) and β3 (His101 of CAS1 and His112 of CAS2), as well as surrounding loops (Asp47 and Cys104 of CAS1; Asp58 and Cys115 of CAS2) (Fig. 4). The C-terminal subdomain is dominated by α-helices flanking on one side the convex surface of the β-sheet, whereas the other side is involved in dimer and homotetramer formation.

Structural comparison of CAS1 and CAS2

The two CAS proteins are closely related isoforms, structurally very similar, and share an overall amino acid sequence identity of 37% (Fig. 5). Only minor differences were evident between the two compared CAS structures. The most striking difference concerns coordination of the bound metal ion. In both CAS structures, the zinc ion is coordinated primarily by two cysteine and one histidine residues (Cys45, His101 and Cys104 in CAS1; Cys56, His112 and Cys115 in CAS2) (Fig. 4). However, the fourth coordination ligand of the zinc ion is a water molecule in CAS1, which, in the active site of one monomer, is accompanied by two additional water molecules separated by a distance of 2.7 Å from each other (Fig. 4A). By contrast, the fourth coordination position of zinc ion in CAS2 is occupied by a carboxylate oxygen atom of the conserved Asp58 (Fig. 4B). In both enzymes, the conserved aspartic acid is part of an Asp/Arg pair proposed to be involved in proton shuffling [12] and catalysis [15]. This amino acid pair is in close proximity to the active core (Fig. 4) and is conserved in all β-CAs analyzed to date [15,27,37]. The different zinc coordination environments at the active site of CAS1 and CAS2 have been observed previously in CAs and have been termed type-I and type-II [38,39].

Discussion

The genome of the filamentous ascomycete *S. macrospora* encodes four carbonic anhydrases. Two β-CAs, named CAS1 and CAS2, were shown to be the major CAs involved in sexual development and ascospore germination [8]. In the present study, we show that both proteins were able to restore growth in a β-CA *S. cerevisiae* deletion mutant at ambient air, demonstrating their *in vivo* activity (Fig. 1). CAS1 and CAS2 were heterologously expressed in *E. coli* for structural and functional studies. Purified CAS1 and CAS2 exhibited hydration activity, although this was low compared to α- and β-CAs from other organisms (Table 1). Filamentous fungi such as *S. macrospora* have evolved a redundant system comprising multiple CAs that can replace each other if needed [8,23,32,40]. By contrast, bacteria or ascomycetous yeasts must often maintain the supply of bicarbonate with a single CA. Therefore, individual CAs from multi-enzyme organisms may exhibit low *in vitro* activity, although overall activity may be higher than that of bacteria or yeast with a single CA enzyme. In support of this, *S. macrospora* single CA deletion mutants are still able

Table 2. Inhibition constants of anionic inhibitors against α-CA isozymes derived from human (hCA II) and bacterial (from the thermophilic bacterium *Sulfurihydrogenibium yellowstonense*, SspCA) sources, as well as the β-CA from a bacterium (*Helicobacter pylori*) HpyCA, the plant *F. bidentis* isoform 1 (FbiCA 1) and *S. macrospora* enzymes CAS1 and CAS2 at 20 °C (pH 8.3) by a stopped flow CO_2 hydrase assay [71]. Errors were in the range of 3–5% of the reported values from three different assays.

	K_I [mM]					
	hCA II[a]	SspCA[b]	HpyCA[c]	FbiCA 1[d]	CAS1[e]	CAS2[e]
F^-	> 300	41.7	0.67	0.71	> 100	> 100
Cl^-	200	8.30	0.56	0.74	9.2	> 100
Br^-	63	49.0	0.38	0.67	9.3	> 100
I^-	26	0.86	0.63	0.71	8.6	7.7
CNO^-	0.03	0.80	0.37	0.93	0.90	0.82
SCN^-	1.60	0.71	0.68	0.83	5.4	5.6
CN^-	0.02	0.79	0.54	0.62	0.94	0.75
N_3^-	1.51	0.49	0.80	0.46	> 100	6.1
HCO_3^-	85	33.2	0.50	0.66	6.5	5.5
CO_3^{2-}	73	39.3	0.42	0.84	> 100	8.8
NO_3^-	35	0.86	0.78	0.78	> 100	> 100
NO_2^-	63	0.48	0.67	0.57	> 100	> 100
HS^-	0.04	0.58	0.58	0.86	0.89	8.5
HSO_3^-	89	21.1	0.63	55.3	3.3	7.3
SnO_3^{2-}	0.83	0.52	0.48	0.53	4.3	0.92
SeO_4^{2-}	112	0.57	0.65	24.5	2.4	9.2
TeO_4^{2-}	0.92	0.53	0.45	0.90	2.5	6.3
$P_2O_7^{4-}$	48.50	0.69	0.75	0.83	3.1	0.96
$V_2O_7^{4-}$	0.57	0.66	0.18	0.66	> 100	1.4
$B_4O_7^{2-}$	0.95	0.67	0.68	0.86	6.7	6.9
ReO_4^-	0.75	0.80	0.82	0.52	8.2	> 100
RuO_4^-	0.69	0.69	1.10	26.1	3.9	> 100
$S_2O_8^{2-}$	0.084	84.6	0.93	0.87	5.0	> 100
$SeCN^-$	0.086	0.07	0.97	0.88	2.9	9.3
CS_3^{2-}	0.0088	0.06	0.21	0.06	0.79	> 100
$Et_2NCS_2^-$	3.1	0.004	0.0074	0.008	0.38	0.93
SO_4^{2-}	> 200	0.82	0.57	0.62	> 100	4.8
ClO_4^-	> 200	> 200	6.50	> 200	> 100	> 100
BF_4^-	> 200	> 200	> 200	> 200	> 100	> 100
FSO_3^-	0.46	0.73	0.75	0.69	0.93	8.4
$NH(SO_3)_2^{2-}$	0.76	0.75	0.70	50.9	0.88	9.2
$H_2NSO_2NH_2$	1.13	0.009	0.072	0.004	0.084	0.048
H_2NSO_3H	0.39	0.042	0.094	0.005	0.069	0.072
Ph-$B(OH)_2$	23.1	0.041	0.073	0.008	0.009	0.056
Ph-AsO_3H_2	49.2	0.005	0.092	0.006	0.035	0.054

[a] De Simone and Supuran [34], Supuran *et al.* [76]; [b] De Luca *et al.* [72]; [c] Nishimori *et al.* [73]; [d] Monti *et al.* [74]; [e] Present study.

to grow in ambient air, whereas deletion mutants of bacteria and yeasts encoding only a single CA cannot grow under these conditions [3,8,29,41,42]. Compared to CAs of other organisms, CAS1 and CAS2 are only weakly inhibited by anions and the sulfonamide drug acetazolamide (Tables 1 and 2). The natural habitat of *S. macrospora* is the dung of herbivores, which is an environment rich in carbon, nitrogen and minerals. High levels of resistance against anionic inhibitors such as nitrite and nitrate might be the result of an adaption of *S. macrospora* to its ecological niche in which ions and trace elements are found at high concentrations [43]. Such an adaption has been proposed for bicarbonate resistance of the α-CA VchCA from *Vibrio cholerae* [44].

Recently, there has been increased interest in utilizing CAs for industrial applications such as CO_2 sequestration and biofuel production [45]. Often, CAs used for such applications do not resist the harsh industrial conditions. In particular, the presence of SO_x and NO_x, which are present in flue gases, can pose a problem for enzyme activity [46]. The resistance of *S. macrospora* CAS1 and CAS2 to anionic inhibitors observed in the present study, coupled with

Table 3. Data collection and refinement statistics.

	CAS1	CAS2
Data collection		
Space group	$P2_12_12$	$F222$
a (Å)	70.08	83.00
b (Å)	80.72	93.90
c (Å)	82.35	97.13
Wavelength (Å)	0.91841	0.82661
Resolution (Å)	36.2–2.7 (2.8–2.7)	33.8–1.8 (1.9–1.8)
Observed reflections	46085 (4718)	70137 (10481)
Unique reflections	13277 (1344)	16776 (2441)
Multiplicity	3.5 (3.5)	4.2 (4.3)
Completeness (%)	98.7 (99.7)	99.2 (99.6)
I/σ (σI)	8.2 (2.3)	18.0 (2.4)
R_{merge} (%)[a]	19.1 (71.2)[d]	3.7 (59.9)
CC(1/2)[b]	97.7 (72.4)	100.0/79.3
Refinement		
Resolution (Å)	36.24–2.69	33.77–1.83
R_{work} (%)	20.4 (26.8)	19.1(32.6)
R_{free} (%)[c]	25.1 (31.3)	21.1 (34.1)
Number of atoms/ B average (Å^2)	3146/40.1	1785/48.7
Protein	2983/40.50	1719/48.8
Solvent	160/33.10	65/45.5
Ions	3/46.38	1/32.7
Rmsd from ideal		
Bond length (Å)	0.005	0.010
Bond angles (°)	0.960	1.362
Ramachandran plot (%)		
Favored	99.49	98.10
Outlier	0.00	0.00
Allowed	0.51	1.90
PDB code	4O1J	4O1K

Values given in parentheses refer to the outer shell.

[a] $R_{merge} = \Sigma_{hkl} \Sigma_i |I_i(hkl) - \langle I(hkl)\rangle| / \Sigma_{hkl} \Sigma_i I_i(hkl)$.

[b] Calculated with XSCALE [77].

[c] R_{free} factor calculated for 5% randomly chosen reflections not included in the refinement.

[d] The elevated R_{merge} value is a result of the high background level of the cryosolution and the very small size of the crystal (7 × 7 × 40 μm). For comparison, the nylon loop used for crystal mounting is 20 μm in diameter.

their efficient expression in *E. coli*, makes them good candidates for industrial applications (Table 2).

The monomeric structure of both β-CAs from *S. macrospora* closely resembles that of other β-CAs, with the three core elements (N-terminal arm, α/β core and a C-terminal extension) being present in all [38]. Three amino acids conserved only in plant-like β-CAs (Gln151, Phe179, Tyr205; numbering according to the *Pisum sativum* CA) further confirm the plant-like architecture of CAS1 and CAS2 [23]. The search for the closest structural neighbors of CAS1 using PDBEFOLD [47] identified β-CAs from *S. cerevisiae* (rmsd 1.68 Å, 184 matched Cα, 30% sequence identity) and *P. sativum* (rmsd 1.64 Å, 187 matched Cα, 32% sequence identity). For CAS2, the *S. cerevisiae* (rmsd 1.7 Å, 180 matched Cα, 27% sequence identity) and *E. coli* (rmsd 1.46 Å, 184 matched Cα, 53% sequence identity) β-CAs showed the highest degree of structural similarity.

Despite their importance for fungal growth and pathogenicity, only two fungal β-CAs and one α-CA have been structurally characterized to date [26,27,48]. Although similar in structure and sequence, the fungal β-CAs CAS1 and CAS2 structures determined in the present study revealed unexpected differences compared to the structures of the β-CAs from *C. neoformans* and *S. cerevisiae*. The *S. macrospora* CAS1 and CAS2 are tetrameric (Fig. 2), whereas *S. cerevisiae* and *C. neoformans* β-CAs form dimeric assemblies [26,27]. Nevertheless, tetrameric assemblies of β-CAs have been reported from bacteria and algae as well [49,50].

The N-termini of CAS1 and CAS2 are composed of two perpendicularly oriented α-helices (Fig. 3). Similarly, the N-terminus of *S. cerevisiae* Nce103 is made up of two α-helices shown to be important for activity but not for dimerization [26]. By contrast, the N-terminus of *C. neoformans* Can2 is composed of four antiparallel α-helices that interact with a channel crossing the active-site entrance. Schlicker *et al.* (2009) assumed that this N-terminal extension may be involved in internal regulatory mechanisms, or may mediate interaction with another protein. The N-terminus of the *Candida albicans* β-CA is even more extended than that of Can2, which was only capable of partially complementing the *C. albicans* CA mutant strain (Fig. S1). This led to the assumption that the length of the N-terminus was particularly important for activity [27]. The conformation of the N-terminal region of CAS1 and CAS2 is structurally similar to that of *S. cerevisiae* CA Nce103 and, not unexpectedly, the phenotype of the Δ*nce103* yeast mutant was completely restored by heterologous expression of *cas1* and *cas2* (Fig. 1).

In the electron density map of CAS1, Cys47, His101 and Cys104 can be clearly seen coordinating the zinc ion. Additionally, three water molecules were observed in close vicinity to the active site of one monomer occupying the asymmetric unit. One water molecule is positioned 2.3 Å away from the metal ion and occupies the fourth coordination position (Fig. 4A), whereas the other two are spaced 2.7 Å apart, which is a distance ~ 0.4 Å longer then the spacing between two oxygen atoms in a CO_2 molecule. The distance of 2.3 Å between the water molecule coordinating the zinc ion and one of the water molecules separated by

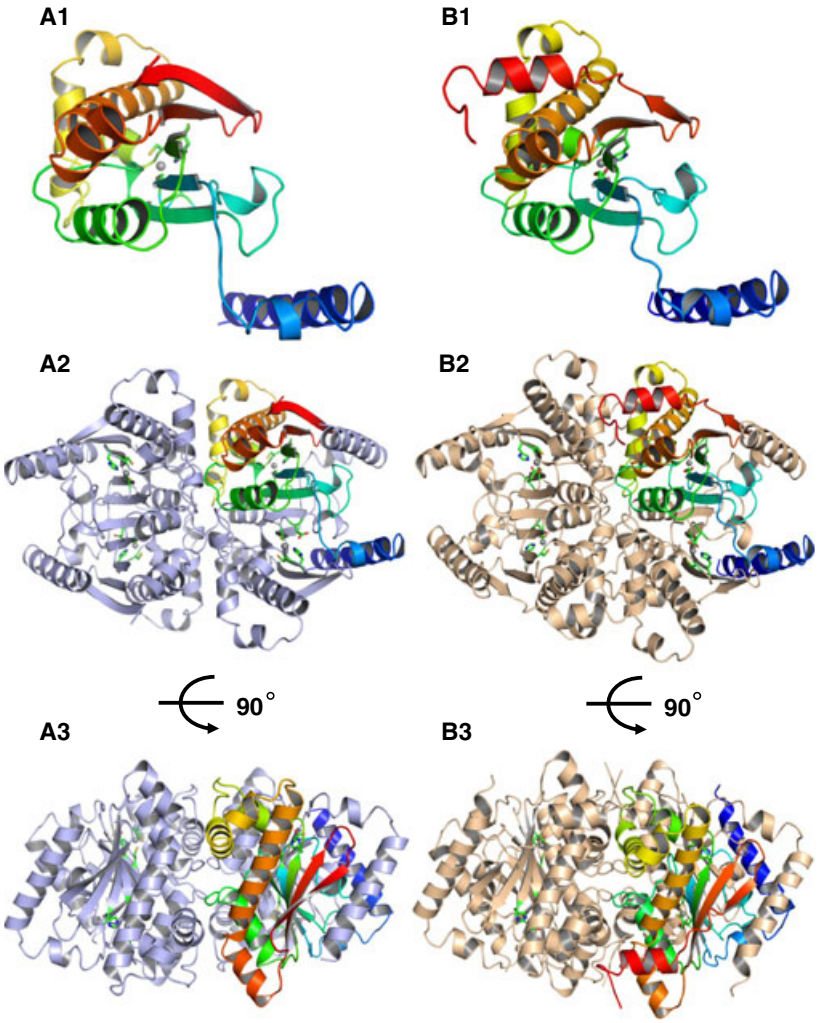

Fig. 2. Crystal structures of carbonic anhydrase CAS1 and CAS2. (A) CAS1. (B) CAS2. (A1, B1) Monomers of CAS1 and CAS2 in cartoon representation (rainbow colored). (A2, B2) Quaternary structure of CAS1 and CAS2 in cartoon representation illustrating the tetrameric assembly. The rainbow-colored monomers are shown in the same orientation as in (A1) and (B1), respectively. (A3, B3) Tetramer of (A2) and (B2) rotated by 90° over the *x*-axis. Zn^{2+} ions are shown as grey spheres. The side chains of the residues coordinating the Zn^{2+} ion are depicted as green sticks for CAS1 and CAS2.

2.7 Å suggests that the latter two could mimic the oxygen atoms of the substrate CO_2 molecule.

A water molecule acting as the fourth ligand coordinating the zinc ion has been already reported for several plant and yeast β-CAs (e.g. the *P. sativum*, *C. neoformans* and *S. cerevisiae* β-CAs) [26,27]. Those structures and the structure of CAS1 reported in the present study represent the so-called open conformation of the enzyme, also named type-I (Fig. 6A) [15,26,27]. By contrast, no water molecules could be localized in the close vicinity of the active site of CAS2. Instead, the coordination sphere of the zinc ion in CAS2 is completed by a carboxylate oxygen atom of conserved Asp58 located on a loop connecting β-strands β1 and β2 in the close proximity to the active site (Fig. 4B). An Asp side chain occupying the fourth position of the zinc coordination sphere has been reported previously for structures of the β-CA from the red alga *Porphyridium purpureum* and bacterial β-CAs from *E. coli*, *Haemophilus influenza* and *Mycobacterium tuberculosis* (Rv3588c) [49,51–53]. The accompanying structural changes of the loop harboring conserved Asp residue cause active site closure and represent the closed (type-II) conformation of the enzyme, which has been shown to be inactive [54] (Fig. 6B). However, the closed conformation of the loop harboring the Asp58 in CAS2 is stabilized by crystal contacts. Therefore, it is anticipated that the observed closed state may convert to an open state when a water molecule replaces the Asp residue at higher pH, such as pH 8.3, at which the kinetic measurements were performed. This phenomenon was demonstrated for the *M. tuberculosis* enzyme Rv1284 [52].

In addition to differences in conformation of the loop responsible for changing the state of the active site (opening and closing), less pronounce differences were observed at the C-termini of *S. macrospora* CAS1 and CAS2. Although CAS1 is nine amino acids longer

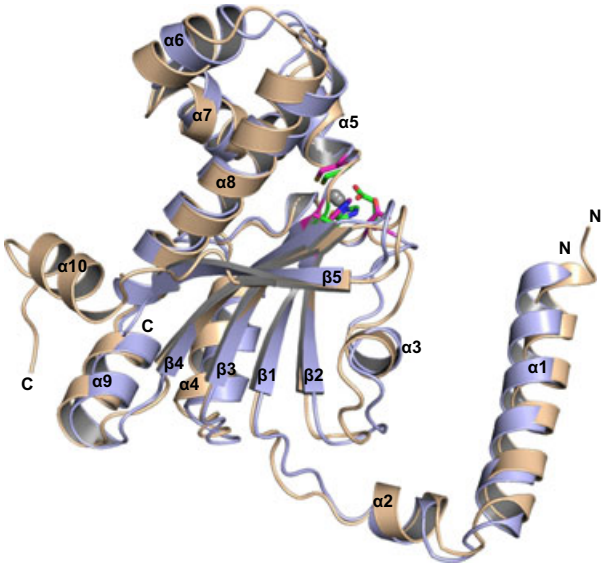

Fig. 3. Superposition of the monomeric ribbon representation for CAS1 (slate blue) and CAS2 (wheat). The secondary structure elements are labeled according to the CAS2 monomer. The first and the last residues of each monomer are labeled N and C. The zinc ions are presented as grey spheres and the zinc coordinating protein residues are depicted as sticks and are colored green (CAS1) and purple (CAS2).

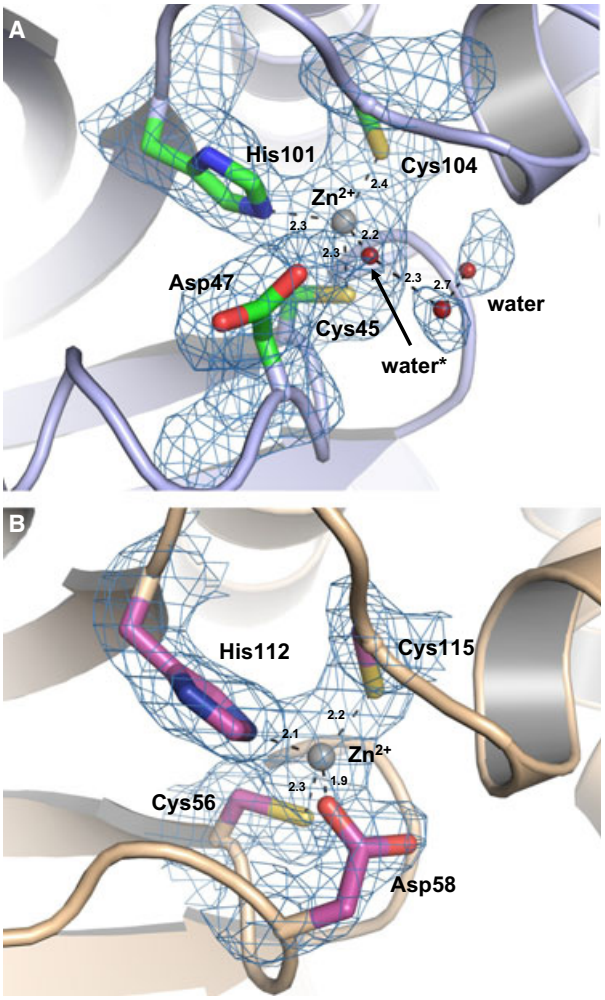

Fig. 4. Active center of CAS1 and CAS2. (A) Coordination of the zinc ion at the active site of CAS1 is achieved by side chains of Cys45, His101 and Cys104. Close to the active center, three water molecules are located. One of these (marked with an arrow and labelled water*) acts as fourth ligand of the Zn^{2+} ion. (B) Side chains of Cys56, His112 and Cys115 coordinate the zinc ion in the active center of CAS2. The fourth position is occupied by Asp58. Distances (Å) are displayed and interactions are indicated by dashed lines. The simulated annealing $mF_o - DF_c$ omit map is contoured at the 3.2 sigma level.

then CAS2, its C-terminal 21 residues could not be localized in the electron density map. By contrast, the C-terminus of CAS2 is almost completely resolved and forms a loop-helix-loop extension, establishing several polar contacts with the adjacent monomer, and thus appears to play an important structural role in the tetramer formation (Fig. S2). This observation can be further confirmed by the structure-based sequence alignment of CAS2 with other dimeric, tetrameric and octameric forms of β-CAs [55], revealing the presence of the loop-helix-loop C-terminal motif only in tetrameric β-CAs (Fig. S3). The dimeric β-CAs either have a short C-terminal tail of a few amino acids or, as in the case of Cab-type CAs from *Methanobacterium thermoautotrophicum* and *M. tuberculosis* Rv1284, terminate with the fifth β-strand of the central β-sheet [27,52,56].

In conclusion, we present for the first time the crystal structures of two β-CA enzymes from a filamentous ascomycete. The monomers of *S. macrospora* CAS1 and CAS2 exhibit high structural similarity to plant-like β-CAs. Both enzymes form tetrameric assemblies, unlike other fungal β-CAs. CAS1 and CAS2 were distinguished by their different active site conformations. CAS1 adopted an 'open' type-I conformation with a water molecule as the fourth ligand coordinating the zinc ion, whereas, in CAS2, a 'closed' type-II conformation was visible in which the conserved Asp residue completed the metal coordination. CAS1 and CAS2 display a high degree of structural similarity to CAs from plant- and human fungal pathogens such as *Fusarium* sp. and *Aspergillus fumigatus* [23]. Inhibition of fungal CAs has attracted attention as a possible treatment for infections caused by fungal pathogens [57,58]. Based on the high sequence identity and structural similarity to β-CAs from other filamentous ascomycetes, the structures of

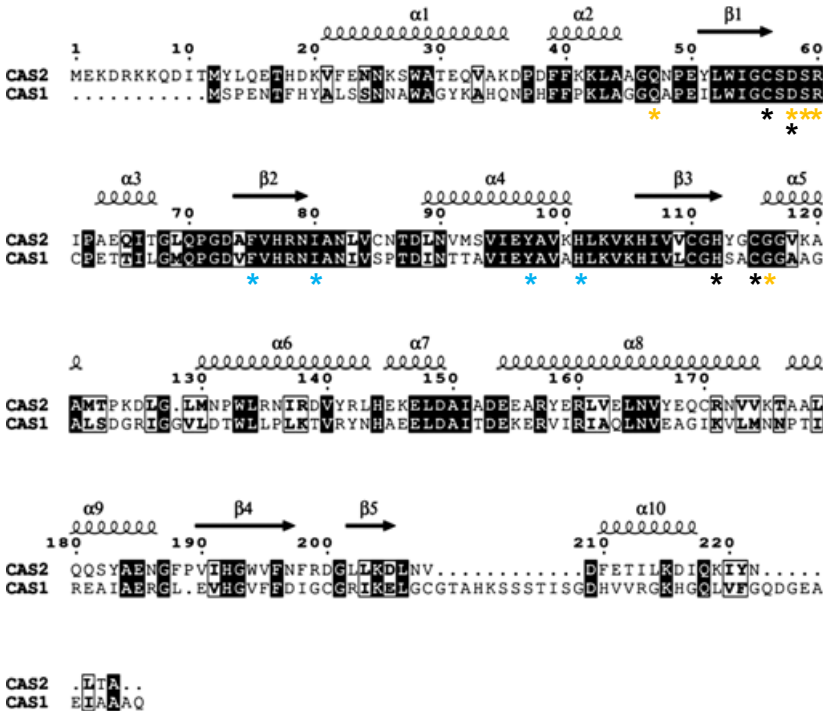

Fig. 5. Amino acid sequence alignment of β-CAs CAS1 and CAS2. The alignment was created with ESPRIPT [75] using the sequences: CAS1 (accession number FM878639) and CAS2 (FM878640). The black asterisks indicate the amino acids involved in zinc binding (Asp58 binds the zinc ion only in CAS2). Conserved amino acids forming the active site are indicated by yellow asterisks and amino acids constituting the active site cleft are highlighted with blue asterisks. Conserved amino acid residues were classified as described previously [38]. Residues identical in both sequences are shaded black, similar amino acids are framed. Positions of secondary structure elements are indicated above the sequence and are based on the CAS2 monomer.

S. macrospora CAS1 and CAS2 reported in the present study might contribute to the development of new antifungal therapeutics.

Materials and methods

In vivo complementation of *S. cerevisiae*

For heterologous complementation of *S. cerevisiae* Δ*nce103* with carbonic anhydrase genes of *S. macrospora*, we used the haploid yeast strain CEN.HE28-h (Table S1). This strain cannot grow under ambient air conditions because a kanamycin resistance cassette replaces the carbonic anhydrase encoding gene *NCE103*. The *heterozygous* diploid yeast deletion strain was incubated on sporulation medium (8.2 $g \cdot L^{-1}$ sodium acetate, 1.9 $g \cdot L^{-1}$ KCl, 0.35 $g \cdot L^{-1}$ $MgSO_4$, 1.2 $g \cdot L^{-1}$ NaCl, 15 $g \cdot L^{-1}$ agar) for 2–4 days at 30 °C. For separation of single spores, the tetrads were resuspended in Zymolyase solution (100 $mg \cdot mL^{-1}$) (Sigma-Aldrich, Germany). After 5 min, the solution was spread as single lane on an YPD [1% (w/v) yeast extract, 2% (w/v) peptone, 2% (w/v) glucose] plate. The spores were isolated with a Micromanipulator (MSM System; Singer Instruments, Watchet, UK) and transferred to a new YPD plate. Only ascospores able to germinate at elevated (5%) CO_2 atmosphere on plates containing 200 $\mu g \cdot mL^{-1}$ G418 sulfate (Roth, Karlsruhe, Germany) were used for the complementation assay. To complement the haploid yeast mutant, the ORF of the two *cas* genes were amplified from wild-type cDNA using the primer pair p426CAS1-f/p426RGSHISCAS1-r for *cas1* and primer pair p426CAS2-f/p426RGSHISCAS2-r for *cas2* (Table S2). The ORF of *cas2* was amplified without the MTS. Using the homologous recombination mechanism of *S. cerevisiae* [59], the PCR fragments (*cas1*: 790 bp, *cas2*: 763 bp) consisting of the corresponding ORF, the 27-bp sequence coding for the RGS6xHis-tag and two 29-bp overhangs to the plasmid were cloned into the *Eco*RI linearized vector p426GAL1 [60] (Table S3). The respective genes are expressed under the control of a galactose inducible promoter of the *GAL1* gene. The constructed plasmids were named p426-CAS1-His and p426-CAS2-His (Table S3). The haploid yeast deletion strain CEN.HE28-h was grown at 5% CO_2 in the Inkubator C42 (Labotect, Rosdorf, Germany) in liquid YPD and transformed with the obtained plasmids using the electroporation method [61]. Transformants were selected on SD-Ura plates containing 200 $\mu g \cdot mL^{-1}$ G418 sulfate at 5% CO_2. For the complementation assay, the cells were grown over night in liquid SD-Ura medium at 5% CO_2 and dropped in 50-μL aliquots in concentrations lasting from 10^6 to 10^1 cells on solid SD- and SG-Ura medium, respectively. The cells were incubated at ambient air and 30 °C. To demonstrate the viability of all cells, a control plate was also incubated at 5% CO_2 and 30 °C. The haploid mutant transformed with the empty vector (CEN.HE28-h + p426GAL1) was used as a negative control. The heterozygous diploid yeast deletion strain transformed with the empty vector (CEN.HE28 + p426GAL1) served as a positive control. To confirm the production of the proteins, a western blot with anti-His serum (Qiagen, Hilden, Germany, 1 : 4000, 1 × NaCl/P_i + 0.5% BSA) was performed.

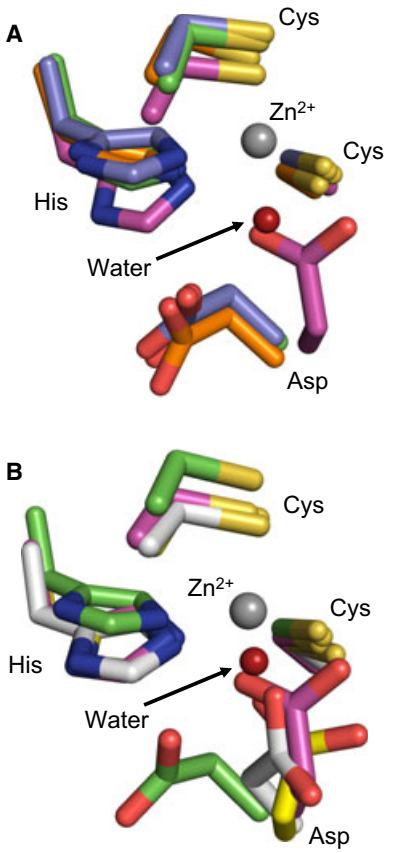

Fig. 6. Superposition of the active site of type-I and type-II plant-like β-CAs. (A) Overlay of the 'open' active site of representative type-I plant β-CAs [*P. sativum* (orange), *C. neoformans* (blue)] with CAS1 (green) and CAS2 (purple). (B) Overlay of the 'closed' active site of representative type-II plant β-CAs [*E. coli* (grey), *P. purpureum* (yellow)] with CAS1 (green) and CAS2 (purple). The zinc ion is shown as a grey sphere. The water molecule in the active center of CAS1 is indicated by a red sphere. [Figure legend corrected on 24 February 2014 after original online publication].

Cloning, expression and purification

The ORF of *cas1* (705 bp) was amplified with primer pair CynT1-pQE_f/CynT1_r (Table S2) and cloned into the *Bam*HI/*Sal*I linearized vector pQE30 (Qiagen). The resulting plasmid pQE30-CAS1 (Table S3) consists of the *cas1* ORF fused in-frame to an N-terminal RGS-6xHis sequence. The *cas2* ORF (678 bp) was amplified without the coding sequence for the mitochondrial target sequence using primer pair CAS2pET22-f/CAS2pET22-r (Table S2) and cloned into the pET22b(+) expression plasmid (Novagen, Madison, WI, USA) linearized with *Nde*I and *Xho*I to create a C-terminal 6xHis fusion protein. The plasmid was named pET-CAS2 (Table S3). The production of both proteins was achieved in *E. coli* strain Rosetta (DE3) (Invitrogen, Carlsbad, CA, USA). The gene expression was induced by the addition of 1 mM isopropyl thio-β-D-galactoside during the exponential phase of growth and lasted for 3–4 h at 30 °C in LB medium supplemented with 0.5 mM $ZnSO_4$. Subsequently, the cells were harvested and resuspended in lysis buffer (20 mM imidazole, 50 mM NaH_2PO_4, pH 8, 300 mM NaCl, 0.02 mM $MgCl_2$, 1 Protease Inhibitor Cocktail Tablet; Roche) and incubated with a spatula-tip amount of lysozyme (Serva, Heidelberg, Germany) and DNase I (AppliChem, Darmstadt, Germany). After 30 min of incubation at 4 °C, the cells were disrupted using a microfluidizer 110S (Microfluidics, Newton, MA, USA). After centrifugation (50 000 ***g*** for 30 min at 4 °C), the clarified lysate was applied on a Ni-NTA agarose column (Qiagen) equilibrated with lysis buffer. Unbound proteins were removed by washing the column with three column volumes of lysis buffer and bound CAS1 or CAS2 were eluted with lysis buffer additionally containing 250 mM imidazole. Elution fractions were analyzed by SDS/PAGE, pooled, concentrated in a Spin-X UF 20 (Corning Inc.) and stored at 4 °C.

Crystallization, data collection and structure determination

CAS1 and CAS2 were crystallized using the sitting-drop vapor diffusion method at 293 K. The droplets were prepared by mixing 1 μL of protein solution (CAS1: 15 mg·mL^{-1}; CAS2: 22 mg·mL^{-1}) and 1 μL of reservoir (CAS1: 0.1 M succinic acid, pH 7, 15% poly(ethylene glycol) 3350; CAS2: 0.1 M Tris-hydrochloride, pH 8.5, 25% poly(ethylene glycol) 4000, 0.2 M $CaCl_2 \times 2H_2O$). Crystals grew within a few days. Before the diffraction experiment, crystals were transferred to cryosolution containing 10% (v/v) glycerol for CAS1 and 5% (v/v) glycerol for CAS2 in addition to the reservoir solution. The oscillation photographs for the CAS1 crystal were collected at beamline 14.1 at the BESSY II (Berlin, Germany) equipped with a Pilatus 6M detector [62]. The diffraction images for CAS2 were collected at beamline P13 equipped with Pilatus 6M detector at the PETRA III (DESY, Hamburg, Germany). The data sets were processed using XDS [63]. Both structures were solved by molecular replacement with PHASER [64] using *E. coli* β-CA [Protein Data Bank (PDB) code: 1I6P [PDB code corrected on 24 February 2014 after original online publication]] and *H. influenzae* β-CA (PDB code: 3E3I) as the search models for CAS1 and CAS2 structures, respectively. In both cases, initial MR solutions were rebuild using Rosetta model completion and relaxation [65]. Manual model completing was performed with COOT [66] alternated with refinement using PHENIX [67]. Data collection and refinement statistics are presented in Table 3. Secondary structure assignment for both structures was carried out using DSSP [68]. Simulated annealing omit map was calculated using CNS [69,70]. Structural figures were generated with PYMOL (http://www.pymol.org).

Size exclusion chromatography and multi-angle laser light-scattering

Four hundred microliters of CAS1 (3.5 mg·mL^{-1}) and 260 μL of CAS2 (2 mg·mL^{-1}) were loaded separately on a 24-mL analytical Superdex 200 (10/300) gel filtration column using an Äkta purifier (GE Healthcare, München, Germany) coupled to a miniDAWN TREOS triple-angle light-scattering detector (Wyatt Technology, Dernbach, Germany). The column was pre-equilibrated with 50 mM NaH_2PO_4 (pH 8), 250 mM imidazole and 300 mM NaCl. Multi-angle laser light-scattering analysis was performed continuously on the column eluate at 291 K (size-exclusion chromatography coupled with multi-angle laser light scattering). Data analysis was carried out using ASTRA (Wyatt Technology).

CA activity and inhibition measurements

A stopped-flow instrument (Applied Photophysics, Leatherhead, UK) was used to assay the CA catalyzed CO_2 hydration activity [71]. Phenol red (0.2 mM) was used as an indicator (absorbance maximum 557 nm), with 10–20 mM TRIS (pH 8.3) as buffer and 20 mM $NaClO_4$ to maintain constant ionic strength. The initial rates of the CA-catalyzed CO_2 hydration reaction were monitored for a period of 10–100 s. The CO_2 concentrations ranged from 1.7 to 17 mM for the determination of kinetic parameters and inhibition constants. For each inhibitor, at least six traces of the initial 5–10% of the reaction were used for determination of the initial velocity. The uncatalyzed rates were determined in the same manner and subtracted from the total observed rates. Stock solutions of inhibitors (10 mM) were prepared in distilled, deionized water. These were diluted up to 0.01 μM with distilled, deionized water. To allow the formation of the E–I complex, inhibitor and enzyme solutions were preincubated together for 15 min at room temperature before the hydration assay. The kinetic parameters for the uninhibited enzymes were determined from Lineweaver-Burk plots. The inhibition constants were obtained by nonlinear least-squares methods using PRISM 3 and the Cheng–Prusoff equation [34,57,72–74]. All reported values represent the mean of at least three different determinations. All inhibitors (sodium salts of the anions and the several small molecules) were commercially available, highest purity compounds, as obtained from Sigma-Aldrich (Milan, Italy).

Acknowledgements

We thank Gertrud Stahlhut for providing excellent technical assistance and Maximillian M. Schütter for help with some experiments. We are grateful to Dr Thomas Monecke for assistance with the size exclusion chromatography and multi-angle laser light-scattering experiments; Claudia Baierlein for isolation of haploid yeast ascospores; and Professor Kai Tittmann for providing access to ultracentrifugation equipment. We thank the BESSY (Berlin) and EMBL/DESY (Hamburg) for access to their beam lines. This work was funded by the Deutsche Forschungsgemeinschaft (PO523/5-1) and partly supported by the Göttingen Graduate School for Neurosciences, Biophysics und Molecular Biosciences (DFG Grants GSC 226/1, GSC 226/2). We thank Britta Herzog and Antonia Jakobshagen for critically reading the manuscript. SP, RL, SE, CS and PN planned the experiments. RL, PN, DV and SE performed the experiments. RL, PN, RF, SP and CS analyzed the data. SP, RF, CS and SE contributed reagents or other essential material. RL, SP, PN and CS wrote the paper.

References

1 Nijhout MM & Carter R (1978) Gamete development in malaria parasites – bicarbonate-dependent stimulation by pH *in-vitro*. *Parasitology* **76**, 39–53.
2 Bahn YS, Cox GM, Perfect JR & Heitman J (2005) Carbonic anhydrase and CO_2 sensing during *Cryptococcus neoformans* growth, differentiation, and virulence. *Curr Biol* **15**, 2013–2020.
3 Klengel T, Liang WJ, Chaloupka J, Ruoff C, Schroppel K, Naglik JR, Eckert SE, Mogensen EG, Haynes K, Tuite MF *et al.* (2005) Fungal adenylyl cyclase integrates CO_2 sensing with cAMP signaling and virulence. *Curr Biol* **15**, 2021–2026.
4 Cummins EP, Selfridge AC, Sporn PH, Sznajder JI & Taylor CT (2013) Carbon dioxide-sensing in organisms and its implications for human disease. *Cell Mol Life Sci* **1**, 15.
5 Hall RA, De Sordi L, MacCallum DM, Topal H, Eaton R, Bloor JW, Robinson GK, Levin LR, Buck J, Wang Y *et al.* (2010) CO_2 acts as a signalling molecule in populations of the fungal pathogen *Candida albicans*. *PLoS Pathog* **6**, e1001193.
6 Cottier F, Leewattanapasuk W, Kemp LR, Murphy M, Supuran CT, Kurzai O & Mühlschlegel FA (2013) Carbonic anhydrase regulation and CO_2 sensing in the fungal pathogen *Candida glabrata* involves a novel Rca1p ortholog. *Bioorg Med Chem* **21**, 1549–1554.
7 Supuran CT (2008) Carbonic anhydrases: novel therapeutic applications for inhibitors and activators. *Nat Rev Drug Discov* **7**, 168–181.
8 Elleuche S & Pöggeler S (2009) β-carbonic anhydrases play a role in fruiting body development and ascospore germination in the filamentous fungus *Sordaria macrospora*. *PLoS ONE* **4**, e5177.
9 Aguilera J, Van Dijken JP, De Winde JH & Pronk JT (2005) Carbonic anhydrase (Nce103p): an essential

biosynthetic enzyme for growth of *Saccharomyces cerevisiae* at atmospheric carbon dioxide pressure. *Biochem J* **391**, 311–316.
10 MacAuley SR, Zimmerman SA, Apolinario EE, Evilia C, Hou Y-M, Ferry JG & Sowers KR (2009) The archetype γ-class carbonic anhydrase (Cam) contains iron when synthesized *in vivo*. *Biochemistry* **48**, 817–819.
11 Lane TW & Morel FMM (2000) A biological function for cadmium in marine diatoms. *Proc Natl Acad Sci USA* **97**, 4627–4631.
12 Tripp BC, Smith K & Ferry JG (2001) Carbonic anhydrase: new insights for an ancient enzyme. *J Biol Chem* **276**, 48615–48618.
13 Hewett-Emmett D & Tashian RE (1996) Functional diversity, conservation, and convergence in the evolution of the α-, β-, and γ-carbonic anhydrase gene families. *Mol Phylogenet Evol* **5**, 50–77.
14 Smith KS & Ferry JG (1999) A plant-type (β-class) carbonic anhydrase in the thermophilic methanoarchaeon *Methanobacterium thermoautotrophicum*. *J Bacteriol* **181**, 6247–6253.
15 Kimber MS & Pai EF (2000) The active site architecture of *Pisum sativum* β-carbonic anhydrase is a mirror image of that of alpha-carbonic anhydrases. *EMBO J* **19**, 1407–1418.
16 Meldrum NU & Roughton FJ (1933) Carbonic anhydrase Its preparation and properties. *J Physiol* **80**, 113–142.
17 Supuran CT (2008) Carbonic anhydrases – an overview. *Curr Pharm Des* **14**, 603–614.
18 Dodgson SJ & Forster RE 2nd (1986) Carbonic anhydrase: inhibition results in decreased urea production by hepatocytes. *J Appl Physiol* **60**, 646–652.
19 Esbaugh AJ & Tufts BL (2006) The structure and function of carbonic anhydrase isozymes in the respiratory system of vertebrates. *Respir Physiol Neurobiol* **154**, 185–198.
20 Alterio V, Hilvo M, Di Fiore A, Supuran CT, Pan P, Parkkila S, Scaloni A, Pastorek J, Pastorekova S, Pedone C *et al.* (2009) Crystal structure of the catalytic domain of the tumor-associated human carbonic anhydrase IX. *Proc Natl Acad Sci USA* **106**, 16233–16238.
21 Whittington DA, Waheed A, Ulmasov B, Shah GN, Grubb JH, Sly WS & Christianson DW (2001) Crystal structure of the dimeric extracellular domain of human carbonic anhydrase XII, a bitopic membrane protein overexpressed in certain cancer tumor cells. *Proc Natl Acad Sci USA* **98**, 9545–9550.
22 Pilka ES, Kochan G, Oppermann U & Yue WW (2012) Crystal structure of the secretory isozyme of mammalian carbonic anhydrases CA VI: implications for biological assembly and inhibitor development. *Biochem Biophys Res Commun* **419**, 485–489.
23 Elleuche S & Pöggeler S (2009) Evolution of carbonic anhydrases in fungi. *Curr Genet* **55**, 211–222.
24 Mogensen E & Mühlschlegel F (2008) CO_2 sensing and virulence of *Candida albicans*. In Human and Animal Relationships (Brakhage A & Zipfel P, eds), pp. 83–94, Springer, Berlin-Heidelberg.
25 Elleuche S & Pöggeler S (2010) Carbonic anhydrases in fungi. *Microbiology* **156**, 23–29.
26 Teng YB, Jiang YL, He YX, He WW, Lian FM, Chen Y & Zhou CZ (2009) Structural insights into the substrate tunnel of *Saccharomyces cerevisiae* carbonic anhydrase Nce103. *BMC Struct Biol* **9**, 67.
27 Schlicker C, Hall RA, Vullo D, Middelhaufe S, Gertz M, Supuran CT, Mühlschlegel FA & Steegborn C (2009) Structure and inhibition of the CO_2 sensing carbonic anhydrase Can2 from the pathogenic fungus *Cryptococcus neoformans*. *J Mol Biol* **385**, 1207–1220.
28 Mogensen EG, Janbon G, Chaloupka J, Steegborn C, Fu MS, Moyrand F, Klengel T, Pearson DS, Geeves MA, Buck J *et al.* (2006) *Cryptococcus neoformans* senses CO_2 through the carbonic anhydrase Can2 and the adenylyl cyclase Cac1. *Eukaryot Cell* **5**, 103–111.
29 Götz R, Gnann A & Zimmermann FK (1999) Deletion of the carbonic anhydrase-like gene *NCE103* of the yeast *Saccharomyces cerevisiae* causes an oxygen-sensitive growth defect. *Yeast* **15**, 855–864.
30 Isik S, Guler OO, Kockar F, Aydin M, Arslan O & Supuran CT (2010) *Saccharomyces cerevisiae* β-carbonic anhydrase: inhibition and activation studies. *Curr Pharm Des* **16**, 3327–3336.
31 Innocenti A, Mühlschlegel FA, Hall RA, Steegborn C, Scozzafava A & Supuran CT (2008) Carbonic anhydrase inhibitors: inhibition of the beta-class enzymes from the fungal pathogens *Candida albicans* and *Cryptococcus neoformans* with simple anions. *Bioorg Med Chem Lett* **18**, 5066–5070.
32 Elleuche S (2011) Carbonic anhydrases in fungi and fungal-like organisms - functional distribution and evolution of a gene family. In Evolution of Fungi and Fungal-like Organisms (Pöggeler S & Wöstemeyer J, eds), pp. 257–274, Springer, Berlin Heidelberg.
33 Clark D, Rowlett RS, Coleman JR & Klessig DF (2004) Complementation of the yeast deletion mutant DeltaNCE103 by members of the beta class of carbonic anhydrases is dependent on carbonic anhydrase activity rather than on antioxidant activity. *Biochem J* **379**, 609–615.
34 De Simone G & Supuran CT (2012) (In)organic anions as carbonic anhydrase inhibitors. *J Inorg Biochem* **111**, 117–129.
35 Vullo D, Sai Kumar RS, Scozzafava A, Capasso C, Ferry JG & Supuran CT (2013) Anion inhibition studies of a β-carbonic anhydrase from *Clostridium perfringens*. *Bioorg Med Chem Lett* **23**, 6706–6710.
36 Krissinel E & Henrick K (2007) Inference of macromolecular assemblies from crystalline state. *J Mol Biol* **372**, 774–797.

37 Cronk JD, O'Neill JW, Cronk MR, Endrizzi JA & Zhang KY (2000) Cloning, crystallization and preliminary characterization of a beta-carbonic anhydrase from *Escherichia coli*. *Acta Crystallogr D Biol Crystallogr* **56**, 1176–1179.
38 Rowlett RS (2010) Structure and catalytic mechanism of the β-carbonic anhydrases. *Biochim Biophys Acta* **1804**, 362–373.
39 Rowlett RS (2014) Structure and catalytic mechanism of β-carbonic anhydrases. In Carbonic Anhydrase: Mechanism, Regulation, Links to Disease, and Industrial Applications (Frost SC & McKenna R, eds), pp. 53–76, Springer, Netherlands.
40 Han KH, Chun YH, Figueiredo Bde C, Soriani FM, Savoldi M, Almeida A, Rodrigues F, Cairns CT, Bignell E, Tobal JM *et al.* (2010) The conserved and divergent roles of carbonic anhydrases in the filamentous fungi *Aspergillus fumigatus* and *Aspergillus nidulans*. *Mol Microbiol* **75**, 1372–1388.
41 Hashimoto M & Kato J (2003) Indispensability of the *Escherichia coli* carbonic anhydrases YadF and CynT in cell proliferation at a low CO_2 partial pressure. *Biosci Biotechnol Biochem* **67**, 919–922.
42 Kusian B, Sultemeyer D & Bowien B (2002) Carbonic anhydrase is essential for growth of *Ralstonia eutropha* at ambient CO_2 concentrations. *J Bacteriol* **184**, 5018–5026.
43 Madejón P, Domínguez M & Murillo J (2012) Pasture composition in a trace element-contaminated area: the particular case of Fe and Cd for grazing horses. *Environ Monit Assess* **184**, 2031–2043.
44 Vullo D, Isik S, Del Prete S, De Luca V, Carginale V, Scozzafava A, Supuran CT & Capasso C (2013) Anion inhibition studies of the α-carbonic anhydrase from the pathogenic bacterium *Vibrio cholerae*. *Bioorg Med Chem Lett* **23**, 1636–1638.
45 González JM & Fisher SZ (2014) Carbonic anhydrases in industrial applications. In Carbonic Anhydrase: Mechanism, Regulation, Links to Disease, and Industrial Applications (Frost SC & McKenna R, eds), pp. 405–426, Springer, Netherlands.
46 Bond GM, Stringer J, Brandvold DK, Simsek FA, Medina MG & Egeland G (2001) Development of integrated system for biomimetic CO_2 sequestration using the enzyme carbonic anhydrase. *Energy Fuels* **15**, 309–316.
47 Krissinel E & Henrick K (2004) Secondary-structure matching (SSM), a new tool for fast protein structure alignment in three dimensions. *Acta Crystallogr D Biol Crystallogr* **60**, 2256–2268.
48 Cuesta-Seijo JA, Borchert MS, Navarro-Poulsen JC, Schnorr KM, Mortensen SB & Lo Leggio L (2011) Structure of a dimeric fungal α-type carbonic anhydrase. *FEBS Lett* **585**, 1042–1048.
49 Cronk JD, Endrizzi JA, Cronk MR, O'Neill JW & Zhang KY (2001) Crystal structure of *E. coli* beta-carbonic anhydrase, an enzyme with an unusual pH-dependent activity. *Protein Sci* **10**, 911–922.
50 Huang S, Hainzl T, Grundstrom C, Forsman C, Samuelsson G & Sauer-Eriksson AE (2011) Structural studies of beta-carbonic anhydrase from the green alga Coccomyxa: inhibitor complexes with anions and acetazolamide. *PLoS ONE* **6**, e28458.
51 Mitsuhashi S, Mizushima T, Yamashita E, Yamamoto M, Kumasaka T, Moriyama H, Ueki T, Miyachi S & Tsukihara T (2000) X-ray structure of beta-carbonic anhydrase from the red alga, *Porphyridium purpureum*, reveals a novel catalytic site for CO_2 hydration. *J Biol Chem* **275**, 5521–5526.
52 Covarrubias AS, Larsson AM, Högbom M, Lindberg J, Bergfors T, Björkelid C, Mowbray SL, Unge T & Jones TA (2005) Structure and function of carbonic anhydrases from *Mycobacterium tuberculosis*. *J Biol Chem* **280**, 18782–18789.
53 Cronk JD, Rowlett RS, Zhang KYJ, Tu C, Endrizzi JA, Lee J, Gareiss PC & Preiss JR (2006) Identification of a novel noncatalytic bicarbonate binding site in eubacterial β-carbonic anhydrase. *Biochemistry* **45**, 4351–4361.
54 Covarrubias AS, Bergfors T, Jones TA & Hogbom M (2006) Structural mechanics of the pH-dependent activity of beta-carbonic anhydrase from *Mycobacterium tuberculosis*. *J Biol Chem* **281**, 4993–4999.
55 Holm L & Rosenström P (2010) Dali server: conservation mapping in 3D. *Nucleic Acids Res* **38**, W545–W549.
56 Strop P, Smith KS, Iverson TM, Ferry JG & Rees DC (2001) Crystal structure of the 'cab'-type β-class carbonic anhydrase from the archaeon *Methanobacterium thermoautotrophicum*. *J Biol Chem* **276**, 10299–10305.
57 Supuran CT (2010) Carbonic anhydrase inhibition/activation: trip of a scientist around the world in the search of novel chemotypes and drug targets. *Curr Pharm Des* **16**, 3233–3245.
58 Supuran CT (2012) Structure-based drug discovery of carbonic anhydrase inhibitors. *J Enzyme Inhib Med Chem* **27**, 759–772.
59 Colot HV, Park G, Turner GE, Ringelberg C, Crew CM, Litvinkova L, Weiss RL, Borkovich KA & Dunlap JC (2006) A high-throughput gene knockout procedure for *Neurospora* reveals functions for multiple transcription factors. *Proc Natl Acad Sci USA* **103**, 10352–10357.
60 Mumberg D, Müller R & Funk M (1994) Regulatable promoters of *Saccharomyces cerevisiae*: comparison of transcriptional activity and their use for heterologous expression. *Nucleic Acids Res* **22**, 5767–5768.
61 Becker DM & Lundblad V (2001) Introduction of DNA into yeast cells. *Curr Protoc Mol Biol Chapter* Chapter 13, Unit13 7.

62 Mueller U, Darowski N, Fuchs MR, Förster R, Hellmig M, Paithankar KS, Pühringer S, Steffien M, Zocher G & Weiss MS (2012) Facilities for macromolecular crystallography at the Helmholtz-Zentrum Berlin. *J Synchrotron Radiat* **19**, 442–449.
63 Kabsch W (2010) Xds. *Acta Crystallogr D Biol Crystallogr* **66**, 125–132.
64 McCoy AJ, Grosse-Kunstleve RW, Storoni LC & Read RJ (2005) Likelihood-enhanced fast translation functions. *Acta Crystallogr D Biol Crystallogr* **61**, 458–464.
65 DiMaio F, Terwilliger TC, Read RJ, Wlodawer A, Oberdorfer G, Wagner U, Valkov E, Alon A, Fass D, Axelrod HL *et al.* (2011) Improved molecular replacement by density- and energy-guided protein structure optimization. *Nature* **473**, 540–543.
66 Emsley P, Lohkamp B, Scott WG & Cowtan K (2010) Features and development of Coot. *Acta Crystallogr D Biol Crystallogr* **66**, 486–501.
67 Adams PD, Afonine PV, Bunkoczi G, Chen VB, Davis IW, Echols N, Headd JJ, Hung LW, Kapral GJ, Grosse-Kunstleve RW *et al.* (2010) PHENIX: a comprehensive Python-based system for macromolecular structure solution. *Acta Crystallogr D Biol Crystallogr* **66**, 213–221.
68 Kabsch W & Sander C (1983) Dictionary of protein secondary structure: pattern recognition of hydrogen-bonded and geometrical features. *Biopolymers* **22**, 2577–2637.
69 Brunger AT (2007) Version 1.2 of the crystallography and NMR system. *Nat Protoc* **2**, 2728–2733.
70 Brunger AT, Adams PD, Clore GM, DeLano WL, Gros P, Grosse-Kunstleve RW, Jiang JS, Kuszewski J, Nilges M, Pannu NS *et al.* (1998) Crystallography & NMR system: a new software suite for macromolecular structure determination. *Acta Crystallogr D Biol Crystallogr* **54**, 905–921.
71 Khalifah RG (1971) The carbon dioxide hydration activity of carbonic anhydrase. I Stop-flow kinetic studies on the native human isoenzymes B and C. *J Biol Chem* **246**, 2561–2573.
72 De Luca V, Vullo D, Scozzafava A, Carginale V, Rossi M, Supuran CT & Capasso C (2012) Anion inhibition studies of an α-carbonic anhydrase from the thermophilic bacterium *Sulfurihydrogenibium yellowstonense* YO3AOP1. *Bioorg Med Chem Lett* **22**, 5630–5634.
73 Nishimori I, Minakuchi T, Kohsaki T, Onishi S, Takeuchi H, Vullo D, Scozzafava A & Supuran CT (2007) Carbonic anhydrase inhibitors: the beta-carbonic anhydrase from *Helicobacter pylori* is a new target for sulfonamide and sulfamate inhibitors. *Bioorg Med Chem Lett* **17**, 3585–3594.
74 Monti SM, De Simone G, Dathan NA, Ludwig M, Vullo D, Scozzafava A, Capasso C & Supuran CT (2013) Kinetic and anion inhibition studies of a β-carbonic anhydrase (FbiCA 1) from the C4 plant *Flaveria bidentis*. *Bioorg Med Chem Lett* **23**, 1626–1630.
75 Gouet P, Robert X & Courcelle E (2003) ESPript/ENDscript: extracting and rendering sequence and 3D information from atomic structures of proteins. *Nucleic Acids Res* **31**, 3320–3323.
76 Supuran CT (2010) Carbonic anhydrase inhibitors. *Bioorg Med Chem Lett* **20**, 3467–3674.
77 Karplus PA & Diederichs K (2012) Linking crystallographic model and data quality. *Science* **336**, 1030–1033.

Supporting information

Additional supporting information may be found in the online version of this article at the publisher's web site:

Fig. S1. Amino acid sequence alignment of β-CAs of different species.

Fig. S2. Detailed view on the C-terminal loop-helix-loop extension of CAS2 and polar contacts to the adjacent subunit.

Fig. S3. Structure-based sequence alignment of CAS2 with nine other β-Cas.

Table S1. Strains used in the present study.

Table S2. Oligonucleotides used in the present study.

Table S3. Plasmids used in the present study.